

DOI: 10.1002/cssc.201301193

# Three-Dimensional Graphitized Carbon Nanovesicles for High-Performance Supercapacitors Based on Ionic Liquids

Chengxin Peng,<sup>[a]</sup> Zubiao Wen,<sup>[b]</sup> Yao Qin,<sup>[a]</sup> Lukas Schmidt-Mende,<sup>[c]</sup> Chongzhong Li,<sup>[e]</sup> Shihe Yang,<sup>[d]</sup> Donglu Shi,<sup>[a]</sup> and Jinhu Yang<sup>\*[a]</sup>

Three-dimensional nanoporous carbon with interconnected vesicle-like pores (1.5–4.2 nm) has been prepared through a low-cost, template-free approach from petroleum coke precursor by KOH activation. It is found that the thin pore walls are highly graphitized and consist of only three to four layers of graphene, which endows the material with an unusually high specific surface area (2933 m<sup>2</sup>g<sup>-1</sup>) and good conductivity. With such unique structural characteristics, if used as supercapacitor electrodes in ionic liquid (IL) electrolytes, the graphitized carbon nanovesicle (GCNV) material displays superior per-

formance, such as high energy densities up to 145.9 Wh kg<sup>-1</sup> and a high combined energy-power delivery, and an energy density of 97.6 Wh kg<sup>-1</sup> can be charged in 47 s at 60 °C. This demonstrates that the energy output of the GCNV-based supercapacitors is comparable to that of batteries, and the power output is one order of magnitude higher. Moreover, the synergistic effect of the GCNVs and the IL electrolyte on the extraordinary performance of the GCNV supercapacitors has been analyzed and discussed.

## Introduction

Supercapacitors, a class of electric double layer capacitors (EDLCs), can store energy by physically adsorbing opposing electrolyte charges in two closely packed electrodes to deliver a significantly higher power density (~10 kW kg<sup>-1</sup>) than batteries (usually <1 kW kg<sup>-1</sup>), which makes them promising as power devices for various portable consumer electronic devi-

ces, uninterruptable power supplies, energy-efficient industrial equipment, electric and hybrid electric vehicles, and power grid applications.<sup>[1–9]</sup> However, the energy density (~5 Wh kg<sup>-1</sup>) of supercapacitors is much lower than that of batteries (26–34 Wh kg<sup>-1</sup> for lead acid batteries and 100–180 Wh kg<sup>-1</sup> for lithium ion batteries). This limits their applications to devices that require both high power and energy. Therefore, current efforts in the development of supercapacitors focus mainly on the improvement of the energy density while maintaining a high power density to match the demand for applications.

As the electrical energy of EDLCs ( $E$ ) is calculated by Equation (1):

$$E = 1/2 CU^2 \quad (1)$$

in which  $U$  is the working voltage, which depends on the electrochemical stability of the electrolytes, and  $C$  is the capacitance, decided essentially by the properties of the electrode materials.<sup>[10]</sup> The strategies for high-energy performance are usually through two approaches, that is, by exploiting materials with enhanced capacitance or by employing electrolytes with high electrochemical stability. According to Equation (2):

$$C = \epsilon_r \epsilon_0 A / 4\pi d \quad (2)$$

in which  $\epsilon_r$  is the electrolyte dielectric constant,  $\epsilon_0$  is permittivity of a vacuum,  $A$  is the electrode specific surface area, and  $d$  is the effective thickness of the electric double layer, it can be deduced that a larger specific surface area of the electrodes leads to a higher charge storage capacity. From this viewpoint, a variety of porous carbonaceous materials that include activated carbons (ACs),<sup>[11–14]</sup> mesoporous carbons,<sup>[15–19]</sup> carbon aer-

[a] Dr. C. Peng,<sup>†</sup> Dr. Y. Qin, Prof. D. Shi, Prof. J. Yang  
Department of Chemistry  
Institute for Biomedical Engineering & Nano Science  
Tongji University  
Shanghai 200092 (P.R. China)  
Fax: (+86)21-65983706  
E-mail: yangjinhu2010@gmail.com

[b] Dr. Z. Wen<sup>†</sup>  
College of Chemistry and Chemical Engineering  
Jiangxi Normal University  
Nanchang 330022 (P.R. China)

[c] Prof. L. Schmidt-Mende  
Department of Physics  
University of Konstanz  
Konstanz (Germany)

[d] Prof. S. Yang  
Nano Science and Technology Program  
Department of Chemistry  
William Mong Institute of Nano Science and Technology  
The Hong Kong University of Science and Technology  
Clear Water Bay, Kowloon, Hong Kong (P.R. China)

[e] Prof. C. Li  
Key Laboratory for Ultrafine Materials of Ministry of Education  
School of Materials Science and Engineering  
East China University of Science and Technology  
Shanghai 200237 (P.R. China)

[†] These authors contributed equally to this work.

 Supporting Information for this article is available on the WWW under <http://dx.doi.org/10.1002/cssc.201301193>.

ogels,<sup>[20,21]</sup> and carbide-derived carbons<sup>[22,23]</sup> have been widely adopted as electrode materials for EDLCs because of their advantages of high surface areas as well as excellent chemical stability and relatively low cost. Usually, compared with mesoporous/macroporous carbon materials, microporous carbons possess a higher specific surface area (SSA) and can achieve higher capacitances. However, these are often realized in aqueous electrolytes because the micropores are only accessible to small aqueous electrolyte ions.<sup>[4]</sup> Consequently, despite high capacitances, the energy densities of these supercapacitors based on microporous materials are not satisfactory because of the narrow electrochemical window ( $U < 1$  V) of aqueous electrolytes. Moreover, as a result of the poor ion transport of narrow micropores, the capacitances as well as energy densities decrease sharply at high charge/discharge rates if a high power uptake is needed.

However, ionic liquids (IL) are ideal electrolytes for supercapacitors because of their unique properties such as high thermal stability and nonflammability, which can improve the working temperature range and safety of supercapacitors,<sup>[24,25]</sup> and especially, wide electrochemical windows of 3–4 V, which can contribute greatly to the energy density of supercapacitors [Eq. (1)]. However, if ILs are used as electrolytes for supercapacitors, the carbon materials require larger mesopores (2–3 nm) to match the IL ions for free access, distortion, and insertion/desertion during cycling.<sup>[26]</sup> This is usually at the expense of the SSA (A) of carbon materials ( $SSA < 2000 \text{ m}^2 \text{ g}^{-1}$ ),<sup>[26–28]</sup> and thereby leads to a low capacitance [Eq. (2)] and energy density of the system [Eq. (1)]. Therefore, the development of new structured carbon materials with a large IL ion-compatible pore size and a high SSA simultaneously is crucial for supercapacitors to obtain both high energy and power density. However, this still remains a great challenge.

In this work, a 3D nanoporous carbon that consists of interconnected vesicle-like pores (1.5–4 nm) has been prepared through the heat treatment of a petroleum coke precursor with KOH as an activation agent. The nanovesicle walls are ultrathin and are made of three to four layers of graphene. In addition, the as-synthesized graphene nanovesicles (GCNVs) exhibit an ultrahigh SSA of  $2933 \text{ m}^2 \text{ g}^{-1}$ , which is approximately double that of normal mesoporous carbon materials ( $< 2000 \text{ m}^2 \text{ g}^{-1}$ ). As expected, the GCNVs display a superior performance such as high energy densities of  $83 \text{ Wh kg}^{-1}$  at  $30^\circ\text{C}$  and  $97 \text{ Wh kg}^{-1}$  at  $60^\circ\text{C}$ , which are comparable to that batteries, with respective power densities of 15 and  $7.5 \text{ kW kg}^{-1}$ , which are one order of magnitude higher than that of batteries, even at a high current density of  $9.6 \text{ A g}^{-1}$ . To the best of our knowledge, this result is among the best comprehensive performances that have been reported for capacitors based on porous carbon materials. The key to success is ascribed to the structural characteristics of the GCNVs, such as a fully accessible high SSA for electrolyte ion adsorption, vesicle-like quasisopores that match the IL ion size for the direct access of the IL ions, as well as good electronic conductivity for rapid ion transport, which contribute synergistically to the high energy and power densities.

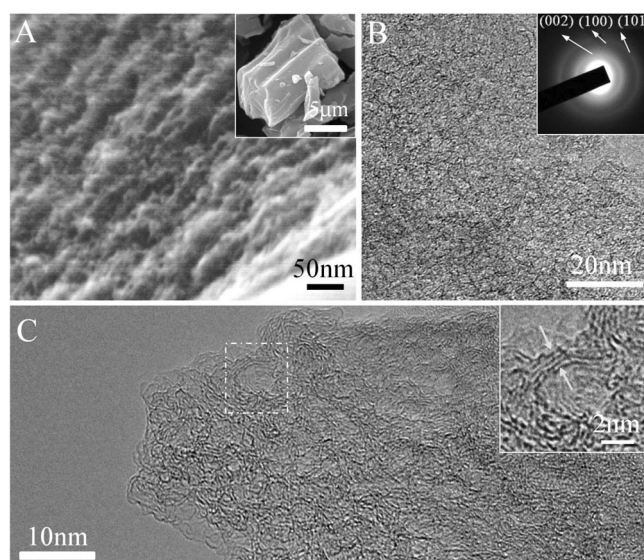


**Figure 1.** A) SEM, B) TEM, and C) HRTEM images of the GCNVs. The inset in A is a low-magnification SEM image of the GCNV material. The inset in B is the corresponding ED pattern of the area observed in B. The inset in C shows the typical structure of a GCNV labeled within the square in C.

## Results and Discussion

A typical SEM image of the GCNV material is shown in Figure 1A. The GCNV particles exhibit an irregular shape with a size of approximately  $15 \mu\text{m}$ , accompanied by some fragments that stand on the surface (inset in Figure 1A). The high-magnification image shows clearly that the particle surface is very rough and consists of a layer of densely distributed nanofoams with sizes estimated to be several nanometers. A typical TEM image obtained from the edge region of a particle is presented in Figure 1B, in which a number of nanopores with circle-like outlines can be observed, which suggests the porous texture of the material. The electronic diffraction (ED) pattern (inset in Figure 1B) that corresponds to the area observed in Figure 1B gives a set of diffraction rings that can be readily assigned to the (002), (100), and (101) planes, respectively, of the hexagonal structure of carbon (carbon, JCPDS 25-0284), which reveals that the material is crystalline with a graphitized structure. From the high-resolution TEM images shown in Figure 1C and Figure S1, it is observed that the nanopores have sizes mainly less than 5 nm with very thin walls composed of two to four layers of graphene, which is well exemplified by an individual pore, the wall of which is composed of four layers of graphene (inset in Figure 1C). The structure of the multiple layers of graphene with a curved shape can also be reflected in the corresponding Raman spectrum (Figure 2A). The Raman spectrum shows two prominent peaks at  $\tilde{\nu} = 1341.3$  and  $1594.5 \text{ cm}^{-1}$  that match the well-documented D and G peaks for graphene materials.<sup>[13b]</sup> The broadening of the D peak implies considerable bond disorder or defects, which is caused by the curved graphene.<sup>[13b]</sup> These multiple-wall pores are reminiscent of vesicles in cell biology, that is, they are ordered assemblies with a multiple-layer structure, formed by amphiphilic molecule self-assembly and responsible for the efficient intra-

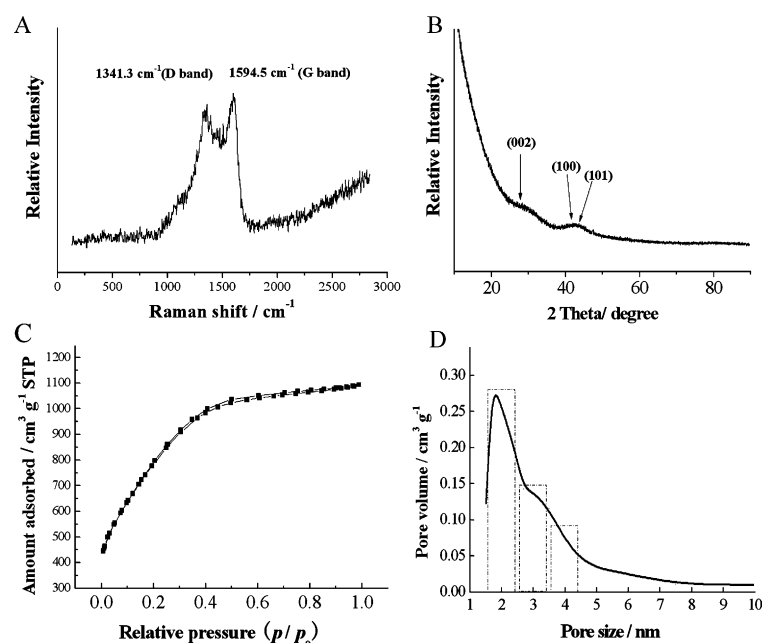


**Figure 2.** A) Raman spectrum, B) XRD pattern, and C) nitrogen adsorption–desorption isotherm with D) the corresponding pore size distribution curve of the GCNV material.

cellular/extracellular mass exchange through their interfaces. The XRD pattern of the as-prepared GCNV materials (Figure 2B) displays broad diffraction peaks that correspond to the (002), (100), and (101) planes of graphitized carbon (JCPDS card no. 25-0284), in good agreement with TEM analysis and the ED result shown in Figure 1B. In addition, the BET measurement (Figure 2C) reveals that the GCNV material is nanoporous with an ultrahigh SSA of  $2933 \text{ m}^2 \text{ g}^{-1}$  and a high pore volume of  $1.692 \text{ m}^3 \text{ g}^{-1}$  (Table S1). Importantly, the pore size distribution curve in Figure 2D indicates that the nanopores have a narrow size distribution (1.5–4 nm) centered at approximately 1.8 nm.

Evidently, the pores are interconnected throughout the entire material after the GCNV formation as they are created by KOH activation from the outer surface to the interior of the petroleum coke precursor.<sup>[29]</sup> Therefore, although they have larger quasi-mesopores, the unusually high SSA of the material should be ascribed to the ultrathin pore walls, the quite uniform pore distribution, and the high pore population density over the material. Notably, the preparation of 3D carbon materials with well-defined pore shapes has been reported from different approaches that include the template method. For example, onion-like carbon from nanodiamonds,<sup>[27]</sup> cage-like carbon from MgO templating,<sup>[28]</sup> 3D macroporous graphene from PS spheres,<sup>[30]</sup> ordered mesoporous carbons from soft pluronic F127,<sup>[16b]</sup> microporous nanographene through sol–gel polymerization,<sup>[13b]</sup> and macroporous graphene foams through a leavening process.<sup>[18b]</sup> These materials are either microporous with a high SSA (up to  $3000 \text{ m}^2 \text{ g}^{-1}$ ) or meso-/macroporous with a low SSA ( $< 2000 \text{ m}^2 \text{ g}^{-1}$ ). As analyzed above, these materials are not favorable for high-performance supercapacitors from the viewpoint of applications (see more discussion in the Supporting Information). In contrast, the 3D GCNV material

that contains quasi-mesopores and an ultrahigh SSA is unusual. The structure of the GCNV material depends highly on the synthetic parameters. For example, a slight change in the amount of KOH or activation temperature in our synthesis will result in the formation of two separate regions of pore distribution and a sharp decrease of the SSA (Figure S2 and Table S1). We consider that a moderately high temperature at the appropriate mass ratio (2.5–3.5) of KOH to the precursors is crucial for the quasi-mesopore formation. However, as carbon activation is a very complex process, it is difficult to determine a clear correlation between the carbon structure and the system parameters.<sup>[9b]</sup> To the best of our knowledge, this is the first time that a carbon material that possesses a larger pore size (quasi-mesopore) and an ultrahigh SSA with a unique vesicle-like pore structure has been prepared. With an optimal combination of pore size and SSA, the GCNV material is expected to serve as a promising electrode material for high-performance supercapacitors as discussed above.

As a classic IL with van der Waals radii of 0.76 nm (cations) and 0.33 nm (anions) and a wide electrochemical window of 3.5 V (Figure S3), 1-ethyl-3-methylimidazolium tetrafluoroborate (EMI-BF<sub>4</sub>) was selected as the electrolyte for the GCNV-based supercapacitors. A cyclic voltammetry (CV) test with various cutoff voltages was performed on the GCNVs at a scan rate of  $20 \text{ mV s}^{-1}$  (Figure 3A). All the CV curves give rectangular shapes, which indicates that the supercapacitor based on the GCNVs and EMI-BF<sub>4</sub> is stable at a high operating voltage up to 3.5 V. Therefore, a voltage range of 0–3.5 V was applied to the research system. As the sweep rate is increased from 20 to  $80 \text{ mV s}^{-1}$ , the CV curve cycled with a cutoff voltage of 3.5 V retains a nearly rectangular shape (Figure 3B). The discharge curves of the GCNVs supercapacitor display a nearly linear response at different current densities from  $0.6\text{--}9.6 \text{ A g}^{-1}$  with a corresponding discharge time from 672–19.3 s, respectively (Figure 3C). Both of these results imply a typical double layer capacitive behavior and little contribution of the pseudocapacitive behavior of the GCNV-based supercapacitor. The small peaks ( $\sim 1.25 \text{ V}$ ) in the CV and the slight deviations in discharge curves, as documented previously, are probably caused by trace amounts of oxygen-containing groups on the GCNV surface after activation.<sup>[31]</sup> In addition, the GCNV supercapacitor also exhibits a very good cycling performance. Notably, unlike pseudocapacitors, EDLCs often have a significantly long cycling life ( $> 100\,000$  cycles) because of the absence of Faradaic redox reactions. The galvanostatic charge–discharge curves are completely reproducible during the first 10 cycles (Figure 3D) and give a high retention of over 98% even after the first 2000 cycles at a current density of  $0.9 \text{ A g}^{-1}$  (Figure S4). It can be observed that there is a slight *IR* decrease at the beginning of each discharge, which is possibly from the internal resistance or equivalent series resistance (ESR)<sup>[32,33]</sup> of the GCNVs in the EMI-BF<sub>4</sub> electrolyte. The ESR of the GCNV material is  $4.0 \Omega$  at  $30^\circ \text{C}$  (Figure 4A). This value is comparable to other gra-

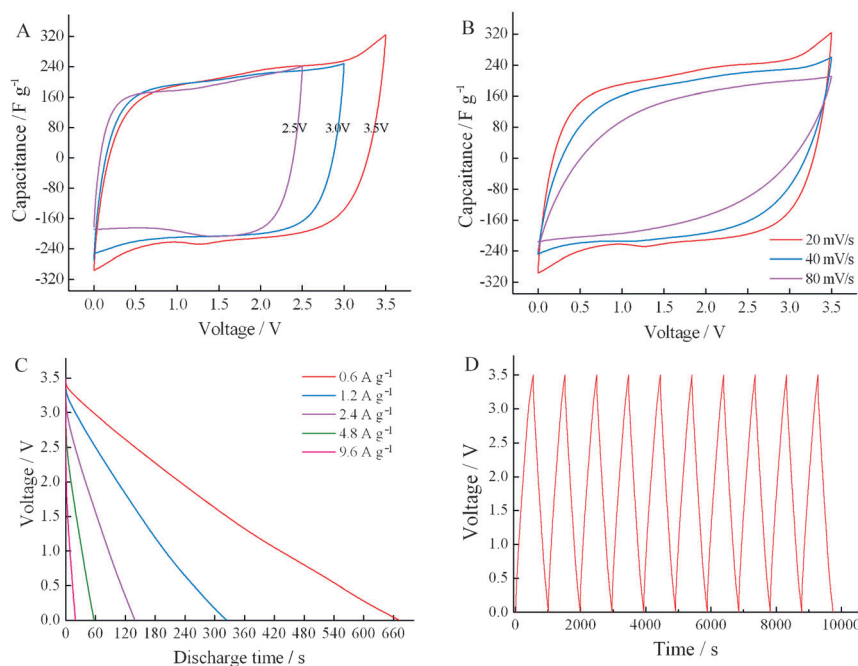


**Figure 3.** Supercapacitor performance of the GCNV material in the EMIBF<sub>4</sub> electrolyte at 30 °C. A) CV curves cycled to different maximum voltages (scan rate: 20 mV s<sup>-1</sup>) and B) CV curves cycled at various scan rates. Rectangular shapes indicate the capacitive behavior. C) Galvanostatic discharge curves of the GCNV-based supercapacitor under different constant currents. D) Charge–discharge performance at 0.9 A g<sup>-1</sup>.

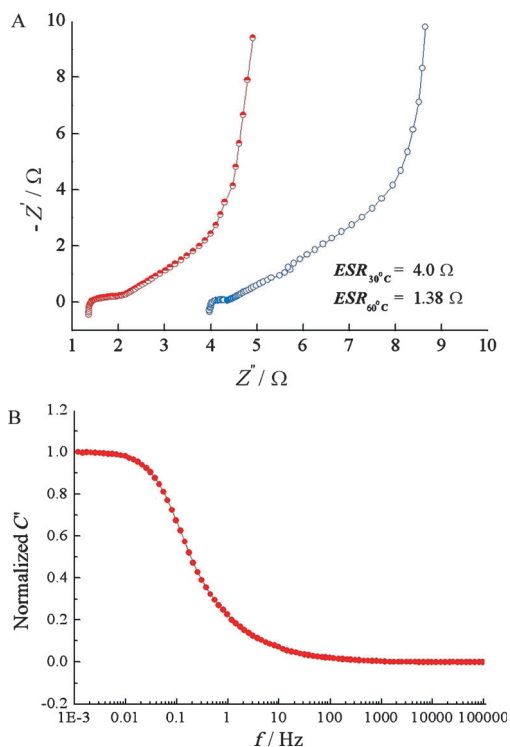


**Figure 4.** A) Nyquist plots of the GCNV electrodes at 30 °C (blue) and 60 °C (red). ESR was decreased from 4.0 to 1.38 Ω if the temperature was increased from 30 to 60 °C. B) Normalized Bode diagrams of the real part of the GCNV-based capacitance versus frequency at 30 °C.

phene-based supercapacitors in the presence of organic or high-viscosity IL electrolytes<sup>[34,35]</sup> owing to the high conductivity of the as-synthesized GCNV material. In addition, the fre-

quency-dependent capacitance of the GCNVs shows that the capacitance decreases sharply by approximately 80% from 0.03 to 1.3 Hz (Figure 4 B). As mesopores are responsive in this range of frequency, this means that the mesopores are mainly responsible for the capacitance. This result also mirrors the BET measurement shown in Figure 2 C and D, which indicates the quasi-mesoporous nature of the GCNV material.

The specific capacitance ( $C_{ss}$ ) at different current densities can be calculated to be 221.3, 214.3, 209.4, 196.6, and 189.7 F g<sup>-1</sup> [see Eq. (S2) in the Supporting Information] in terms of the discharge curves shown in Figure 3 C, which shows a downward tendency with increasing current density from 0.6 to 9.6 A g<sup>-1</sup> (Figure 5 A). The corresponding energy and power

densities are further calculated according to Equations (S2) and (S3), as shown in Figure 5 B, in which energy densities of 94.1, 91.2, 89.1, 83.6, and 80.7 Wh kg<sup>-1</sup> are achieved with the corresponding power densities of 488, 978.8, 2228.7, 5282.7, and 15047.2 W kg<sup>-1</sup>, respectively. It can be concluded that the GCNV-based supercapacitors are capable of storing a maximum energy density of 94.1 Wh kg<sup>-1</sup> and retaining a high energy of 80.7 Wh kg<sup>-1</sup> at a very high cycling rate with a discharge time of less than 20 s (19.3 s). The values for energy and power density were calculated according to the mass of the GCNV electrode material. Based on a weight ratio of 30% for the active electrode material in the packaged supercapacitor device, a practical energy density for the large-scale GCNV-based supercapacitor of up to 28.2 Wh kg<sup>-1</sup> can be obtained. Compared with other supercapacitors based on carbon materials with IL electrolytes, the GCNV supercapacitor is able to deliver higher energies at the same current densities applied. For example, as shown inset in Figure 5 B, the energy densities of the GCNV supercapacitor are close to or even outperform current graphene supercapacitors<sup>[31,34,35]</sup> and are more than twice as high as supercapacitors based on porous carbon<sup>[32,36]</sup> or carbon nanotubes.<sup>[37,38]</sup> Therefore, GCNV supercapacitors have not only a higher energy output than current graphene-based devices but can also be fabricated at a lower cost. Furthermore, the improved performance of the GCNV-based supercapacitor can be obtained at higher operating temperatures. If we elevated the temperature to 60 °C, higher capacitances of 343.0, 301.9, 262.8, and 229 F g<sup>-1</sup> were obtained at current densities of 1.2, 2.4, 4.8, and 9.6 A g<sup>-1</sup>, respectively (Figure 5 C), which is ascribed to the high thermal stability and decreased resistance of the GCNV supercapacitor (Figure 4 A). Consequently, higher

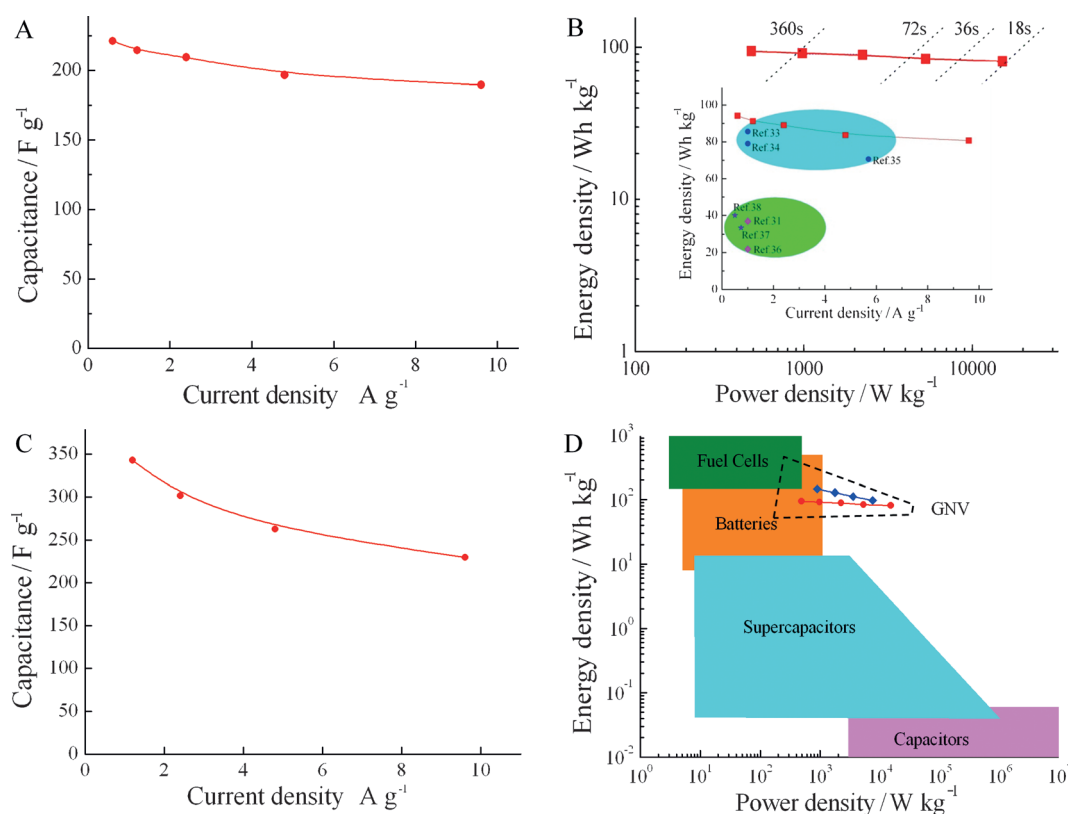


**Figure 5.** Specific capacitance of GCNVs in EMI-BF<sub>4</sub> at different specific currents at A) 30 and C) 60 °C, B) Ragone plot for GCNV electrode with 3.5 V cutoff voltages, and D) performance comparison between several different energy storage devices.<sup>[3]</sup> Inset of B shows the performance comparison of energy density versus current density between the GCNV and other supercapacitors based on carbon materials. The GCNV electrode presented in this study shows higher energy densities than most other supercapacitors and higher power densities than batteries and fuel cells (D).

energy densities that range from 145.9–97.6 Wh kg<sup>-1</sup> can be delivered at 60 °C with discharge times of 588–47 s (Figure S5), which means that, for the GCNV-based supercapacitor, a maximum energy density of 145.9 Wh kg<sup>-1</sup> can be stored and even a high energy density of 97.6 Wh kg<sup>-1</sup> can be recharged in less than 1 min (47 s). For a packaged cell, a maximum energy density above 43 Wh kg<sup>-1</sup> can be expected. The Ragone plots of several main energy storage devices that include traditional capacitors, supercapacitors, batteries, and fuel cells<sup>[3]</sup> are shown in Figure 5D, which gives a comparison of their combinative performances. It can be seen that the GCNV-based supercapacitor can provide a high energy uptake, which approaches that of batteries and even fuel cells, while retaining a high power output, which is one order of magnitude higher than that of batteries. The high energy-power output with a high operating temperature and electrochemical stability will endow the GCNV-based supercapacitors with an optimistic prospect for many important practical applications.

To further investigate the influence of the pore size of the ACs on their electrochemical performance, two control carbon samples (samples A and B, see Figure S2 and Table S1) with separate pore size distributions in the micro- and mesopore regions were adopted as supercapacitor electrodes for comparison. It can be seen that besides mesopores of around 2 nm, there are smaller micropores (<1.5 nm) and bigger mesopores (~4 nm) in the control samples (Figure S2). The electrodes

based on samples A and B show respective ESR values of 6.2 and 3.7 Ω, which are comparable to that of GCNVs (Figure S6). However, compared with the GCNV system, the CV curves of the two electrodes conducted at various voltage scan rates display twisted rectangular shapes (Figure 6A and B). In addition, as shown in Figure 6C, the specific capacitances are much lower than that of the GCNV electrode at the same current densities. As a result of the lower capacitance, the energy densities of the supercapacitors based on the control samples are decreased greatly to 20–60 Wh Kg<sup>-1</sup>, which is 30–60% of that of the GCNVs. Notably, an excellent power output can also be achieved (Figure 6D) because of the existence of larger mesopores (~4 nm), which is conducive to the diffusion of the IL ions. The decrease of the capacitance and the energy deterioration are considered to be caused by incompatibility between the IL ions and the pore sizes of the control samples. As discussed above, the small micropores (<1.5 nm) may block the free entrance of IL ions, and the bigger mesopores (~4.0 nm) allow more IL ions to get into the pores, which result in the formation of incomplete double layers or disordered multiple layers within the pores rather than EDLs. The high compatibility between the pore size and IL ions is crucial for the formation of effective EDLs with a minimal thickness (*d*) and the full availability of SSA (*A*), which thus allows the high capacitance [Eq. (2)] and energy density [Eq. (1)].

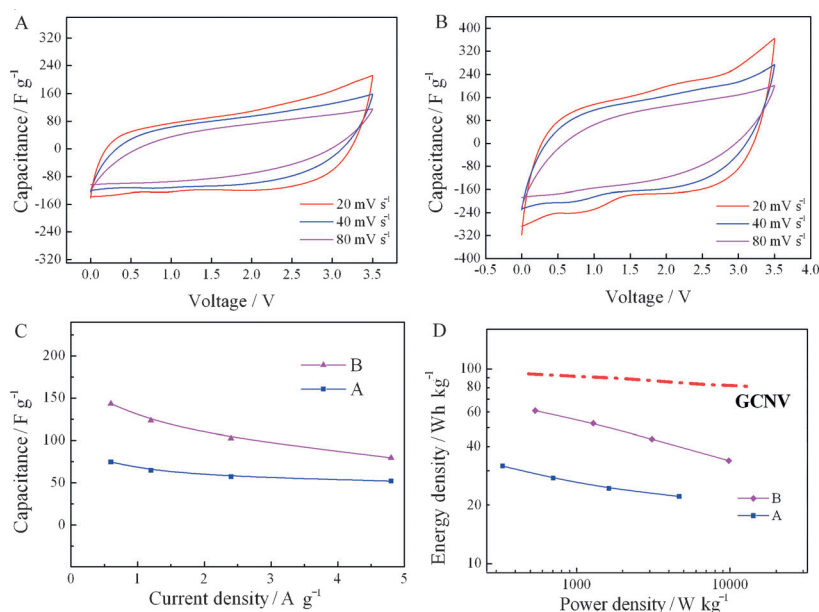


**Figure 6.** CV curves of A) sample A and B) sample B cycled at various scan rates, and C and D) the specific capacitance of these two control samples in EMI-BF<sub>4</sub> at different specific currents at 30 °C.

The interaction between IL ions and the GCNVs on the electrode material interface is illustrated in Figure 7 (upper right), in which IL ions can insert freely into the electrode material through the 3D interconnected GCNV nanopores to form effective EDLs on the interface of the GCNVs. A charged GCNV is shown tentatively as an example to simulate the spherical EDL structure with positive holes on the GCNV walls and negative BF<sub>4</sub><sup>-</sup> ions inside the GCNVs (lower left), respectively. We think

the superior performance of the GCNV-based supercapacitor can be ascribed to the unique structure of the GCNVs. As illustrated in Figure S7, firstly, the ultrahigh SSA of the GCNVs provides abundant active sites for electrolyte ion adsorption, which leads to the high capacitance and energy density. Secondly, the thin graphitized walls with high electronic conductivity are beneficial to IL ion delivery into the full inner surface of the 3D GCNVs. This facilitates the ion transport and makes the SSA fully available, which are crucial for both high energy and high power density. Thirdly, the quasi-mesopores of the GCNVs with IL ion-compatible size,<sup>[26,39]</sup> serve as not only an effective pathway towards the fully porous GCNVs, but also local reservoirs for IL ions to form effective monolayers, responsible for the high power and energy density as well. It has been proposed that, for porous carbon materials, small pores (< 1.5 nm) would hinder IL ion insertion and only 2–3 nm or bigger pores guarantee IL ion monolayer formation.<sup>[26]</sup> Furthermore, the theoretical simulation of the IL system showed a capacitance increase with increasing pore size from 1.1 to 1.3 nm,<sup>[39]</sup> which indicates the tendency of increasing capacitance with increasing pore width in the quasi-mesopore region.

These investigations also confirm that our quasi-mesoporous GCNV material is not only appropriate for the EDL formation of IL ions, but also feasible to acquire high capacitance. Last, the utilization of ILs endows the device with a high operating temperature, and especially, wide electrochemical window, which contributes greatly to the high energy density. Notably, aside from the points discussed above regarding the influence on the supercapacitor performance, ion behavior in the confined space of nanopores that leads to multilayered or incomplete double-layered structures may also be addressed for consideration.<sup>[29]</sup> To better understand the ion behavior within the carbon nanopores, in situ characterization techniques and computational modeling are required.

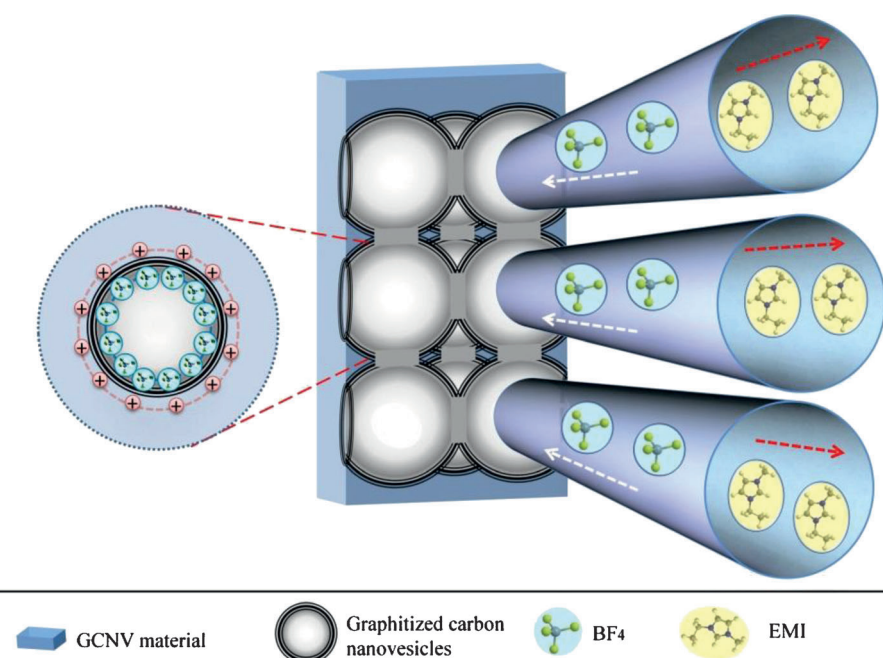


**Figure 7.** Schematic illustration of the interaction between the GCNVs and IL ions on the interface of the GCNV electrode. The lower left shows the simulation of a charged GCNV that forms a spherical EDL that consists of two layers of opposite charges (positive holes: red, negative BF<sub>4</sub><sup>-</sup>: blue) on the GCNV walls and inside the GCNVs, respectively.

## Conclusions

Three-dimensionally interconnected graphitized carbon nanovesicles (GCNVs) have been prepared from a petroleum coke precursor by heat treatment with KOH. The GCNVs exhibit a narrow pore distribution (1.5–4 nm) centered at 1.8 nm and ultrathin graphitized walls with a thickness of two to four layers of graphene, which leads to an unusually high SSA of 2933 m<sup>2</sup>g<sup>-1</sup>. Owing to their unique structural advantages, the GCNVs display a superior performance as supercapacitor electrodes with neat IL electrolytes, such as ultrahigh capacitance (343.0 Fg<sup>-1</sup>) and energy density (145.9 Wh kg<sup>-1</sup>), and high combined energy-power outputs, that is, a stored energy density of 80.7 Wh kg<sup>-1</sup> can be recharged in 20 s at 30 °C and a higher value of 97.6 Wh kg<sup>-1</sup> can be recharged in 47 s at 60 °C. Therefore, the GCNV-based supercapacitors are capable of delivering high energy as batteries and, simultaneously, high power as supercapacitors. The results demonstrate that our high-quality reproducible GCNVs are an improved material for a new generation of supercapacitors with low cost, high stability, and especially high energy and power density. Moreover, the GCNV material also has great potential as efficient electrodes for lithium ion batteries<sup>[40,41]</sup> and as conductive supports for visible photocatalysis<sup>[42]</sup> and sensors,<sup>[43]</sup> if loaded with functional counterparts such as metals or metal oxides. These related investigations are underway.

## Experimental Section

### Preparation of GCNVs

The pretreated petroleum coke precursors from Xinjiang Xintai Zhongli Company were firstly ground to approximately 28 mesh, heated to 400 °C at a ramping rate of 10 °C min<sup>-1</sup>, and precarbonized at this temperature for 1 h in a tubular furnace under a N<sub>2</sub> atmosphere. After it was cooled to RT naturally, the precarbonized AC was ground to 180 mesh and soaked in KOH solution at a certain weight ratio with stirring for 12 h. Then the mixture was dried, heated to 800 °C at a heating speed of 10 °C min<sup>-1</sup>, and held for 20 min to accomplish the activation process. After it was washed with 1 mol L<sup>-1</sup> HCl, the pH of the solution was adjusted to neutral (pH ≈ 6–7) with distilled water. Finally, the GCNV product was obtained after the mixture was washed by ethanol and dried at 120 °C for 8 h.

### Material characterization

The structure of the GCNV material was characterized by SEM (JEOL, JSM-6700F and Hitachi, S-4800), high-resolution transmission electron microscopy (HRTEM, JEM 2011, 200 kV), and power XRD by using a D/max2550VB3+/PC X-ray diffractometer with CuK<sub>α</sub> radiation with a 1.5418 Å wavelength. The BET specific surface area (*S*<sub>BET</sub>) of the powders was analyzed by N<sub>2</sub> adsorption in a Tristar 3000 nitrogen adsorption apparatus at 77 K. Raman spectra were recorded by using a spectrophotometer (XploRA, Horiba Jobin Yvon) with a 532 nm laser.

### Device assembly

EMI-BF<sub>4</sub> (purchased from Lanzhou Institute of Chemical Physics, CAS) was treated with molecular sieves (4 Å) for 2 days before use. The electrodes were prepared by mixing the samples, carbon black, and polytetrafluoroethylene (PTFE) in a mass ratio 80:10:10. The mixture was dispersed in ethanol and sonicated adequately to form a slurry. Then it was coated onto a nickel foam current collector (diameter = 10 mm), pressed at 8 MPa, and dried under vacuum at 120 °C for 24 h to form an active film with a thickness of approximately 100 μm. The final mass on each electrode is 8.1 mg. Prior to cell assembly, the prepared electrodes were soaked in the IL at 40 °C for 12 h under vacuum to enhance the wettability between the electrode materials and the ILs. The cells were assembled in an Ar-filled glove box with water and oxygen contents both less than 1 ppm.

### Electrochemical testing

The capacitive performance of the samples in the IL were tested by a symmetric two-electrode cell and a glass microfiber filter separator (Whatman, GF/A). CV, galvanostatic charge/discharge (GC) and electrochemical impedance spectroscopy (EIS) measurements were performed by using a CHI 660 workstation (CH Instruments, USA) at ambient temperature. The scan rate of CV was varied from 10–100 mV s<sup>-1</sup> in the range of 0–3.5 V. GC measurements were performed in the current range of 0.1–10 A g<sup>-1</sup>. EIS was recorded by applying the open-circuit potential and an ac oscillation of 5 mV over the frequency range of 100 kHz to 0.001 Hz.

## Acknowledgements

This work was supported financially by the National Natural Science Foundation (21001082, 21273161, and 21101117), The Program for Professor of Special Appointment (Eastern Scholar) at Shanghai Institutions of Higher Learning (No: 2013-13), Shanghai Innovation program (13ZZ026), Scientific Research Foundation for the Returned Overseas Chinese Scholars of SEM, Visiting scholar fund of the Key Laboratory for Ultrafine Materials of Ministry of Education, East China University of Science and Technology, and the Fundamental Research Funds for the Central Universities.

**Keywords:** capacitors · carbon · electrochemistry · ionic liquids · nanostructures

- [1] B. E. Conway, *Electrochemical Capacitors*, Kluwer Academic/Plenum Publishers, New York, 1999.
- [2] M. Inagaki, H. Konno, O. Tanaike, *J. Power Sources* **2010**, *195*, 7880–7903.
- [3] M. Winter, R. J. Brodd, *Chem. Rev.* **2004**, *104*, 4245–4269.
- [4] J. Chmiola, G. Yushin, Y. Gogotsi, C. Portet, P. Simon, P. L. Taberna, *Science* **2006**, *313*, 1760–1763.
- [5] P. Simon, Y. Gogotsi, *Nat. Mater.* **2008**, *7*, 845–854.
- [6] C. Largeot, C. Portet, J. Chmiola, P.-L. Taberna, Y. Gogotsi, P. Simon, *J. Am. Chem. Soc.* **2008**, *130*, 2730–2731.
- [7] J. Chmiola, C. Largeot, P.-L. Taberna, P. Simon, Y. Gogotsi, *Angew. Chem.* **2008**, *120*, 3440–3443; *Angew. Chem. Int. Ed.* **2008**, *47*, 3392–3395.
- [8] D. W. Wang, F. Li, M. Liu, G. Q. Lu, H. M. Cheng, *Angew. Chem.* **2008**, *120*, 379–382; *Angew. Chem. Int. Ed.* **2008**, *47*, 373–376.
- [9] a) B. Xu, F. Wu, R. J. Chen, G. P. Cao, S. Chen, Y. S. Yang, *J. Power Sources* **2010**, *195*, 2118–2124; b) J. C. Wang, S. Kaskel, *J. Mater. Chem.* **2012**, *22*, 23710–23725.

- [10] E. Frackowiak, F. Béguin, *Carbon* **2001**, *39*, 937–950.
- [11] H. Y. Liu, K. P. Wang, H. S. Teng, *Carbon* **2005**, *43*, 559–566.
- [12] B. Xu, F. Wu, D. B. Mu, L. L. Dai, G. P. Cao, H. Zhang, S. Chen, Y. S. Yang, *Int. J. Hydrogen Energy* **2010**, *35*, 632–637.
- [13] a) L. Wei, M. Sevilla, A. B. Fuertes, R. Mokaya, G. Yushin, *Adv. Energy Mater.* **2011**, *1*, 356–361; b) J. Biener, S. Dasgupta, L. H. Shao, D. Wang, M. A. Worsley, A. Wittstock, J. R. I. Lee, M. M. Biener, C. A. Orme, S. O. Kucheyev, B. C. Wood, T. M. Willey, A. V. Hamza, J. Weissmüller, H. Hahn, T. F. Baumann, *Adv. Mater.* **2012**, *24*, 5083–5087.
- [14] X. L. Li, C. L. Han, X. Y. Chen, C. W. Shi, *Microporous Mesoporous Mater.* **2010**, *131*, 303–309.
- [15] S. Álvarez, M. C. Blanco-López, A. J. Miranda-Ordieres, A. B. Fuertes, T. A. Centeno, *Carbon* **2005**, *43*, 866–870.
- [16] a) B. Xu, F. Wu, R. J. Chen, G. P. Cao, S. Chen, Z. M. Zhou, Y. S. Yang, *Electrochim. Commun.* **2008**, *10*, 795–797; b) Y. Lv, F. Zhang, Y. Q. Dou, Y. P. Zhai, J. X. Wang, H. J. Liu, Y. Y. Xia, B. Tu, D. Y. Zhao, *J. Mater. Chem.* **2012**, *22*, 93–99.
- [17] A. B. Fuertes, G. Lota, T. A. Centeno, E. Frackowiak, *Electrochim. Acta* **2005**, *50*, 2799–2805.
- [18] a) J. Jin, S. Tanaka, Y. Egashira, N. Nishiyama, *Carbon* **2010**, *48*, 1985–1989; b) Z. Q. Niu, J. Chen, H. H. Hng, J. Ma, X. D. Chen, *Adv. Mater.* **2012**, *24*, 4144–4150.
- [19] Z. H. Feng, R. S. Xue, X. H. Shao, *Electrochim. Acta* **2010**, *55*, 7334–7340.
- [20] N. Liu, S. Zhang, R. Fu, M. S. Dresselhaus, G. Dresselhaus, *Carbon* **2006**, *44*, 2430–2436.
- [21] J. Li, X. Y. Wang, Y. Wang, Q. H. Huang, C. L. Dai, S. Gamboa, P. J. Sebastian, *J. Non-Cryst. Solids* **2008**, *354*, 19–24.
- [22] J. Leis, M. Arulepp, A. Kuura, M. Lätt, E. Lust, *Carbon* **2006**, *44*, 2122–2129.
- [23] J. Chmiola, G. Yushin, R. Dash, Y. Gogotsi, *J. Power Sources* **2006**, *158*, 765–772.
- [24] L. A. Blanchard, D. Hancu, E. J. Beckman, J. F. Brennecke, *Nature* **1999**, *399*, 28–29.
- [25] M. Armand, F. Endres, D. R. MacFarlane, H. Ohno, B. Scrosati, *Nat. Mater.* **2009**, *8*, 621–629.
- [26] M. Lazzari, F. Soavi, M. Mastragostino, *Fuel Cells* **2010**, *10*, 840–847.
- [27] D. Pech, M. Brunet, H. Durou, P. H. Huang, V. Mochalin, Y. Gogotsi, P.-L. Taberna, P. Simon, *Nat. Nanotechnol.* **2010**, *5*, 651–654.
- [28] K. Xie, X. T. Qin, X. Z. Wang, Y. N. Wang, H. S. Tao, Q. Wu, L. J. Yang, Z. Hu, *Adv. Mater.* **2012**, *24*, 347–352.
- [29] P. Simon, Y. Gogotsi, *Acc. Chem. Res.* **2013**, *46*, 1094–1103.
- [30] B. G. Choi, M. H. Yang, W. H. Hong, J. W. Choi, Y. S. Huh, *ACS Nano* **2012**, *6*, 4020–4028.
- [31] Y. W. Zhu, S. Murali, M. D. Stoller, K. J. Ganesh, W. W. Cai, P. J. Ferreira, A. Pirkle, R. M. Wallace, K. A. Cychosz, M. Thommes, D. Su, E. A. Stach, R. S. Ruoff, *Science* **2011**, *332*, 1537–1541.
- [32] L. Wei, M. Sevilla, A. B. Fuertes, R. Mokaya, G. Yushin, *Adv. Funct. Mater.* **2012**, *22*, 827–834.
- [33] M. D. Stoller, S. Park, Y. Zhu, J. An, R. S. Ruoff, *Nano Lett.* **2008**, *8*, 3498–3502.
- [34] a) C. G. Liu, Z. N. Yu, D. Neff, A. Zhamu, B. Z. Jang, *Nano Lett.* **2010**, *10*, 4863–4868; b) Y. C. Qiu, X. F. Zhang, S. H. Yang, *Phys. Chem. Chem. Phys.* **2011**, *13*, 12554–12558.
- [35] T. Y. Kim, H. W. Lee, M. Stoller, D. R. Dreyer, C. W. Bielawski, R. S. Ruoff, K. S. Suh, *ACS Nano* **2011**, *5*, 436–442.
- [36] M. Rose, Y. Korenblit, E. Kockrick, L. Borchardt, M. Oschatz, S. Kaskel, G. Yushin, *Small* **2011**, *7*, 1108–1117.
- [37] X. L. Wang, G. Li, Z. Chen, V. Augustyn, X. M. Ma, G. Wang, B. Dunn, Y. F. Lu, *Adv. Energy Mater.* **2011**, *1*, 1089–1093.
- [38] Z. Chen, V. Augustyn, J. Wen, Y. W. Zhang, M. Q. Shen, B. Dunn, Y. F. Lu, *Adv. Mater.* **2011**, *23*, 791–795.
- [39] P. Wu, J. S. Huang, V. Meunier, B. G. Sumpter, R. Qiao, *ACS Nano* **2011**, *5*, 9044–9051.
- [40] H. Bai, C. Li, G. Q. Shi, *Adv. Mater.* **2011**, *23*, 1089–1115.
- [41] C. X. Peng, B. D. Chen, Y. Qin, S. H. Yang, C. Z. Li, Y. H. Zuo, S. Y. Liu, J. H. Yang, *ACS Nano* **2012**, *6*, 1074–1081.
- [42] L. Zhao, X. F. Chen, X. C. Wang, Y. J. Zhang, W. Wei, Y. H. Sun, M. Antonietti, M. M. Titirici, *Adv. Mater.* **2010**, *22*, 3317–3321.
- [43] H. B. Yao, G. Huang, C. H. Cui, X. H. Wang, S. H. Yu, *Adv. Mater.* **2011**, *23*, 3643–3647.

---

Received: November 6, 2013

Published online on January 28, 2014